FREQUENCY-DEPENDENT NATURE OF *Pn* IN WESTERN CHINA: GAUSSIAN BEAM MODELING OF DATA FROM THE HI-CLIMB EXPERIMENT

Robert L. Nowack[1], Wang-Ping Chen[2], and Tai-Lin Tseng[2]

Purdue University[1] and University of Illinois[2]

Sponsored by Air Force Research Laboratory

Contract No. FA8718-08-C-0025
Proposal No. BAA08-42

ABSTRACT

In realistic models of the crust and the upper mantle where vertical gradients in wave speeds and major interfaces are present, propagation of *Pn*, an important seismic phase at regional distances, involves complex effects of interference. Such effects can result in wave-trains whose frequency-contents and amplitudes vary with distance in counter-intuitive ways. In this new project, we are investigating the propagation of *Pn* beneath western China using data from Hi-CLIMB (An Integrated Study of the Himalayan-Tibetan Continental Lithosphere during Mountain Building). This experiment is one of the largest broadband seismic experiments to date, with more than 210 deployments at close station-spacing of 3–8 km over a distance of 800 km. The linear array is complemented by a regional array of comparable aperture, producing an unprecedented dataset for Eurasia. For the current project, which just began in May of 2008, we are organizing a dataset for regional seismic events recorded by the Hi-CLIMB arrays and will show examples of long seismic profiles over apertures of 500 km from several different azimuths. We are also investigating methods of modeling and inversion based on Gaussian beams (GB), which offer several distinct advantages. First, GB modeling can be applied both for interference waves, which have caustics, and for pure head waves. Second, GB modeling can handle laterally varying media, an important aspect that cannot be investigated by standard methods such as reflectivity. Third, GB is computationally efficient, suitable for analyzing large datasets. We will illustrate our approaches with data from an earlier experiment using explosions. Based on numerous events recorded by the Hi-CLIMB array, we will investigate frequency-dependent propagation of *Pn* over a large region in western China using GB and also finite-difference schemes. Attributes of seismic wave-trains, including arrival times, amplitudes of signal-envelopes, and instantaneous pulse frequencies will be used to constrain how structures in the crust and the upper mantle affect the propagation of *Pn*. The objective is to achieve self-consistent models of *Pn* propagation in western China which are free from assumptions such as a frequency-independent factor for geometric spreading. To this end, our results should advance efforts in isolating effects of frequency-dependent propagation from those of pure-inelastic attenuation (Q), leading to improved methodologies for discrimination and yield estimates at regional distances.

OBJECTIVES

In this new project, which started in May 2008, we are analyzing the propagation of regional *Pn* waves recorded by Hi-CLIMB (An Integrated Study of the Himalayan-Tibetan Continental Lithosphere during Mountain Building) in Tibet. Considering the dense station-spacing (3 to 8 km) and large aperture (800 km) of the Hi-CLIMB seismic experiment, our objective is the use these densely recorded data to construct a self-consistent model of *Pn* propagation over a large region in western China. In turn, a better understanding of frequency-dependent effects of propagation from data inversion/modeling will improve frequency dependent attenuation models of regional *Pn* phases, leading to a clearer separation of inelastic from elastic effects in a laterally varying crust and upper mantle, eventually eliminating the assumption of a simplified, frequency-independent geometric spreading component.

To account for the intricate nature of *Pn* propagation, we are applying the Gaussian beam (GB) method, an asymptotic approach. GB is stable at caustics and can be used for the diving waves, pure head-waves, and interference waves by choosing suitable beam parameters (Nowack and Stacy, 2002). A major advantage of GB is that it works well in laterally varying media. In contrast, alternatives such as the reflectivity method, are restricted to one-dimensional media. When compared with purely numerical simulations for laterally varying media, such as the finite difference method, GB is computationally efficient in facilitating modeling and inversion of large datasets—tasks in which a large number of forward calculations are required. However, for small scale scattering, hybrid methods or full finite difference modeling may still be required. As a practical measure, essential features of *Pn* waveforms will be distilled into seismic attributes such as arrival times, envelopes of wave amplitudes, and instantaneous pulse frequencies for modeling and inversion.

RESEARCH ACCOMPLISHED

The Hi-CLIMB seismic array was deployed between 2002 and 2005, in three phases, over 210 broadband sites at a station-spacing of 3-8 km (for the main, linear array). The main, north-south trending linear array is complemented by an east-west expanding regional array. The overall the aperture is about 800 km by 800 km (Figure 1). A unique feature of Hi-CLIMB is that it is the only seismic profile that crosses the highest portions of the Himalayas, linking baseline measurements of the Indian shield, in a pristine state prior to its involvement in active deformation, with data in the interior of Tibet. There are abundant, high quality data from numerous events at regional distances from the array. Figure 2 shows a preliminary plot of regional events with magnitudes greater than 4.6 over the time period of the Hi-CLIMB deployment.

Figure 3 shows a preliminary seismic profile from a single event with a magnitude of 4.6 located to the west of the array (located by the star in Figure 2) and recorded by central and northern portions of the Hi-CLIMB array. Clear arrivals of both *Pn* and *Pg* phases are observed to epicentral distances of more than 550 km, with *Pn* overtaking *Pg* as the first arrival at distances near 300 km. The first arrivals are marked by the dotted line, and the *Pn* arrival becomes a first arrival after about 325 km. By comparing the signals marked by box A near 350 km with a dominant frequency of about .5 Hz with box B near 560 km where the pulse frequency is higher at about .7 Hz, this increase in dominant frequency with distance suggests complex interference effects for *Pn* propagation in this region. A preliminary profile from a second event with a magnitude of 4.8 with a location just south of the middle and northern portions of the array is shown in Figure 4. Here, the *Pn* becomes the first arrival after about 290 km. The character of the *Pn* is more complicated for this profile than for the profile for the first event, and this suggests that there is significant lateral variability in the region that will need to be addressed in this study.

To interpret first arrival *Pn* data recorded from regional events by the Hi-CLIMB array, the Gaussian beam method will be used for larger scale features in the model. The Gaussian beam method (GB) is an asymptotic approach for the computation of high-frequency wavefields in laterally varying media by the summation of paraxial beams, each surrounding a central ray-path and having a Gaussian distribution in amplitude away from the central ray (Popov, 1982; Cerveny et al., 1982; Nowack and Aki, 1984). Reviews of the method are given by Babich and Popov (1989) and more recently by Nowack (2003) and Popov (2002). There are several advantages in using GB. First, individual beam components have no singularities along their paths. Thus the summation of beams is also regular everywhere, in contrast to ray methods. Second, GB naturally introduces some smoothing and therefore is not as sensitive to model parameterizations as ray-methods. Third, GB does not require the added computation of two-point ray tracing.

New approaches are being developed to perform two parameter beam summations based on initial position and angle of individual beam components. The advantage of these new approaches is that a wider range of beam parameters can be used for the each individual beam solution, but the trade-off is in speed of computation (Lugara et al., 2003; Nowack, 2003; Nowack et al., 2006; Nowack et al., 2007a; Nowack, 2008).

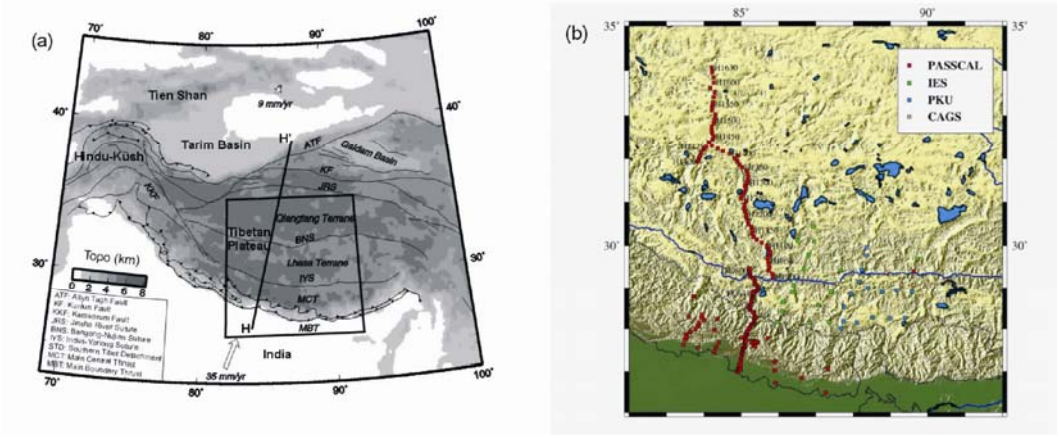

Figure 1. Map showing geologic setting and configuration of Project Hi-CLIMB. (a) Grey-scale topographic map showing overall setting of the Himalayan-Tibetan collision zone. Two open arrows show ground velocity with respect to stable Eurasia. The box shows the region depicted in panel (b). Thin, solid curves show major geological boundaries. (b) Topographic map showing the full configuration of the Hi-CLIMB broadband seismic array. Notice a large aperture of 800 km by 800 km and the dense spacing of stations along the main, linear array. In addition to the IRIS/PASSCAL pool, instruments also came from several other participating institutions (see legend).

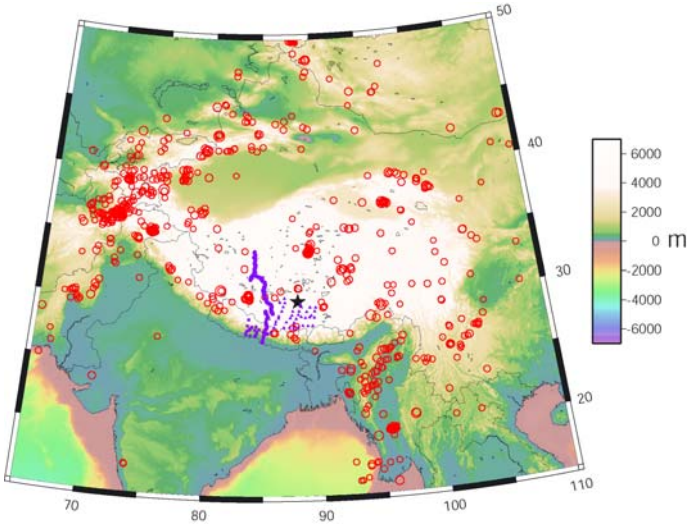

Figure 2. A color-coded topographic map, showing epicenters of large to moderate-sized earthquakes (m_b 4.6 or above; open red circles) recorded by the Hi-CLIMB array (purple triangles). The asterisk marks the epicenter of a Tibetan earthquake (m_b~4.8) which serves as the seismic source of the preliminary profile shown in Figure 4.

To efficiently describe essential features of a complex waveform, it is useful to identify key attributes of the data. Procedures for extracting such attributes include complex trace analysis, and the general approach of wavelet analysis (e.g., Daubechies, 1992; Mallat, 1999). The approach described here is the former, in which an analytic signal is constructed from a seismogram. From the analytic signal, its envelope and instantaneous frequency can be

determined. Applications of complex trace analysis to seismic data have been described by Taner et al. (1979), and an application to estimate seismic attenuation by matching observed values of instantaneous frequency was

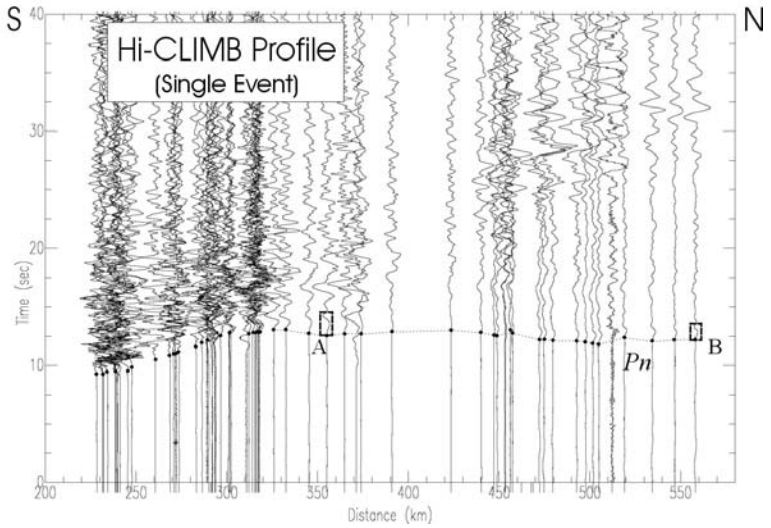

Figure 3. An example of seismic profile from a single event (marked by the star in Figure 2) recorded by central and northern portions of the Hi-CLIMB main array, showing clear arrivals of *Pn* (marked by the dotted curve) which become the first arrival at distances beyond about 325 km. Notice the dominant frequency of *Pn* actually can increase with distance: Compare signals marked by box A, about 0.5 Hz near 350 km; and box B, about 0.7 Hz near 550 km. Solid circles mark first arrivals at selected seismograms. The time-scale is reduced by a wave speed of 8.0 km/s.

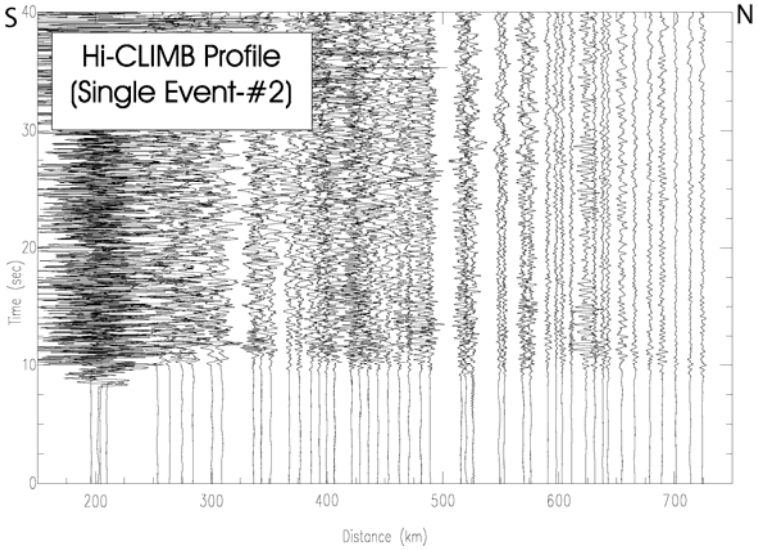

Figure 4. A second example of a seismic profile from a single event with a magnitude of 4.8 located directly south of the middle and northern sections of the Hi-CLIMB array. The *Pn* becomes the first arrival at distances beyond about 290 km. The time-scale is reduced by a wave speed of 8.0 km/s.

performed by Matheney and Nowack (1995). It is important to recall that the instantaneous frequency is generally not equivalent to the spectral frequency. However, an appropriate weighted average of the instantaneous frequency

converges to an average of positive spectral frequencies. Figure 5 shows an example of results from this procedure. For a seismic phase of interest, one can extract amplitudes from its envelope, timing of the seismic phase, and instantaneous frequencies as a function of time. For estimating seismic attenuation, one can match instantaneous frequencies between observed and attenuated reference pulses (Matheney and Nowack, 1995). More general inversions of all seismic attributes for selected seismic phases are also feasible, including previous work by Nowack and Matheney (1997) and Matheney et al. (1997).

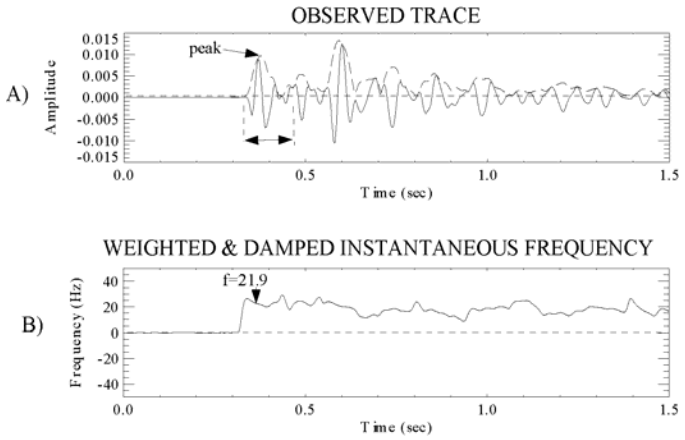

Figure 5. An example of extracting attributes from seismic data. A) Comparison of observed seismogram (solid trace) and its envelope calculated based on the Hilbert transform of data (dashed curve). The peak amplitude of the Hilbert envelope for the first pulse is marked. B) Damped and smoothed instantaneous frequency as a function of time (from Matheney and Nowack, 1995).

Pn is not a simple head-wave but is comprised of complex sets of interfering waves when there is a positive velocity gradient with respect to depth below the Moho interface (Cerveny and Ravindra, 1971; Hill, 1971; Menke and Richards, 1980). These interfering waves can simply result from the spherical nature of the earth (Hill, 1973; Sereno and Given, 1990; Yang et al., 2007), an effect equivalent to a velocity gradient in the corresponding flattened model. How observed amplitudes of refracted arrivals change over distance supports the interpretation that these

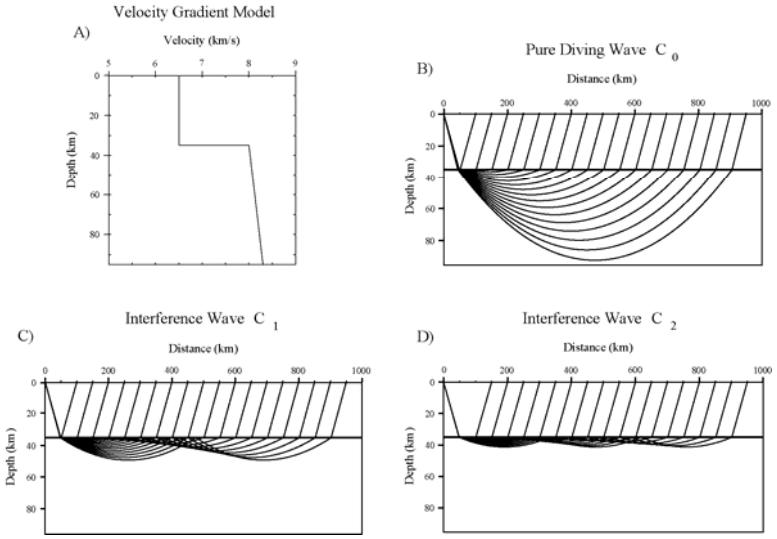

Figure 6. Illustration showing how a positive gradient in wave velocity beneath the Moho can affect the propagation of *Pn*. A) The model for *P*-wave speeds. The linear gradient beneath the Moho can simply arise from the spherical nature of the earth. B) Paths of the primary, diving rays (pure head waves are not shown). C) Paths of the first set of sub-Moho interference wave. D) Paths of the second set of sub-Moho interference wave (from Nowack and Stacy, 2002).

arrivals are comprised of diving and interference waves, instead of only a pure head wave (Braile and Smith, 1975). Figure 6 shows an example of how a positive upper mantle gradient can effect the propagation of Pn waves by forming a set of interference waves at the Moho (from Nowack and Stacy, 2002).

In the last several years, there has been a debate on the effects of small scale scattering in the upper mantle on the propagation of teleseismic *Pn*. Ryberg et al. (1995, 2000) and Tittgemeyer et al. (1996) favored a model in which scattering in the upper mantle can account for many of the characteristics of teleseismic *Pn*. In contrast, Morozov et al. (1998) and Morozov and Smithson (2000) advocated a model with a positive upper mantle gradient forming an interference head wave along with crustal scattering to explain teleseismic *Pn*. However, the recent analysis of Nielson and Thybo (2003) supports the model that the *Pn* phase travels as an upper mantle whispering gallery and that the origin of its long coda at teleseismic distances is due to crustal scattering. For our study, we will model the first arrival *Pn* phase as an interference wave at regional distances using Gaussian beam modeling. At greater distances, a hybrid approach or the direct use of finite difference modeling may be required to model the characteristics of teleseismic *Pn* as a combination of upper mantle gradients and small scale scattering in the crust or upper mantle.

Nowack and Stacy (2002) compared expansions of interference waves using Gaussian beams and the reflectivity method, which is restricted to one-dimensional velocity structures. The fact that GB expansions are non-singular at caustics is essential for multiple underside reflections ,which are associated with caustics and pseudo-caustics, and for these cases finite-sized beams are used. Meanwhile, broad beams are used to represent wide-angle reflections, including the pure head-wave (Nowack and Aki, 1984). In both cases, beams are specified by effective planar phase-fronts at the receiver, providing stable results during summations.

Figure 7 shows comparisons of results from GB and reflectivity, where the reflectivity modeling includes multiples from the free surface which were not included in the GB modeling. In general, these two methods yield comparable results: Notice the good agreement between the two methods in key crustal and *Pn* seismic attributes at all distances. In Fig. 7C, the envelope amplitudes of the first arriving pulses are shown following the procedure of Mathaney and Nowack (1995). The gap near 125 km corresponds to the cross-over distance between the direct crustal arrival and *Pn*. Fig. 7D shows the instantaneous pulse frequencies for the first arrival. At distances less than 100 km, instantaneous pulse frequencies are for the direct, crustal arrivals. At greater distances, the values are for *Pn*. For this particular velocity model, instantaneous frequencies (f_I) initially drop just beyond the cross-over distance, mainly reflecting properties of the pure head-wave. Subsequently, f_I starts recovering as diving and interference waves begin to emerge. f_I continues to increase with distance and eventually overshoots beyond values of direct arrivals seen at close-in distances, an effect resulting from interference of different sets of underside reflections below the Moho. This result is confirmed by analyzing centroid-frequencies of the amplitude spectra of the relevant pulses (Nowack and Stacy, 2002). A similar trend in f_I was reported by Cerveny and Ravindra (1971) using asymptotic analysis. These pure-elastic effects in regional body-waves must be accounted for in order to obtain meaningful estimates of attenuation.

It should be emphasized again that unlike reflectivity, GB is valid for laterally varying media. This is an essential feature to study regional body-waves in areas such as western China where laterally varying structure is most likely to be prevalent in the lithosphere. To this end, we will further validate GB in laterally varying earth models by comparing with other methods which generates complete wavefields, such as the finite difference method (Virieux, 1988). The advantage of using the Gaussian beam method is primarily in its computational speed, a necessary feature for inversion or modeling of massive datasets where a large number of forward simulations must be performed.

The discussed methodologies to be used for Hi-CLIMB were previously applied to data from the Deep Probe/SAREX project by Stacy and Nowack (2002). SAREX (Southern Alberta Refraction Experiment) was designed to provide detailed information on crustal structures along the Canadian portion of the combined Deep Probe/SAREX profile (Clowes et al., 2002; Gorman et al., 2002). To interpret the observations, Stacy and Nowack (2002) computed synthetic seismograms using GB; whose attributes were then compared with those extracted from the data. The resulting features in the amplitudes and the instantaneous frequencies were found to be more complicated than that shown in Figure 7. In addition, a model for Q was simultaneously determined, resulting in a self-consistent representation of both elastic and inelastic effects of wave propagation over a large range of

distances. When modeling Pn propagation beneath Hi-CLIMB in western China, it is anticipated that more complicated *Pn* propagation characteristics will also be found.

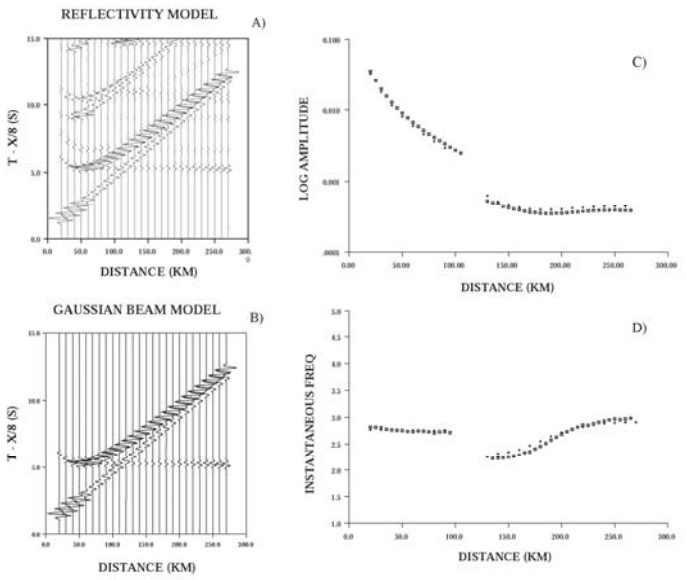

Figure 7 Synthetic seismograms and associated seismic attributes from the simple layer over a gradient model. A) Synthetic seismograms using the reflectivity method. B) Synthetic seismograms using the Gaussian beam method. C) Amplitude of the envelope of the first arriving pulse as a function of distance. Notice that there is a sudden drop in amplitudes near distances of 100 km. Results from Gaussian beam modeling (pluses) and those from reflectivity (squares) are similar. D) Instantaneous frequency of the first arrival pulse as a function of distance. Beyond distance of about 120 km, instantaneous frequency actually increases with increasing distance. Again, results from Gaussian beam modeling (pluses) and those from reflectivity (squares) are similar. The source pulse is a Gabor wavelet with a dominant frequency of 2.77 Hz. To isolate elastic effects of wave propagation, a constant Q value of 2000 was assumed (from Nowack and Stacy, 2002).

A major initial task of the project is to first make a comprehensive database of regional events recorded by the Hi-CLIMB array. The database will include full waveforms, instrument responses, a catalog of events and other important information such as uncertainties of locations and focal mechanisms. Meissner et al. (2004) used earthquake data recorded by the INDEPTH III array in central Tibet to study regional phases and concluded that errors in epicenters of up to 15 km are negligible for *Pn* and would only slightly affect *Pg* at close-in distances. So errors in epicenter do not appear to be a major concern. Nevertheless, we plan to quickly assess such errors by comparing event catalogs based on global (Engdahl, et al., 1998) and regional datasets, both of which are available in the public domain (the latter is available at the China Earthquake Networks Center, CENC). In terms of focal depths, it has been known for some time that most events are shallow in Tibet, between 5 to 10 km (Molnar and Chen, 1983; Chen and Molnar, 1983; Langin et al., 2003). Nonetheless, if necessary, relocations will be performed using a combination of regional data from the Hi-CLIMB array and teleseismic data. One possibility is to adopt a simplified relocation approach, as used by Zhu et al. (2006) for regional events in Tibet.

If necessary, for larger events, m_b of 5.5 and above, we can obtain precise results of source parameters from the inversion of waveforms recorded at teleseismic distances. Similarly, for smaller events, their source parameters can be retrieved from inversion of regional waveforms (Zhu et al., 2006). Both procedures are routinely performed by Chen's group (e.g., Kao et al., 2002; Chen and Yang, 2004). Meanwhile, there are a number of models reported in the literature for the crust and upper mantle of Tibet (e.g., Hearn et al., 2004; Liang et al., 2004, 2006; Sun and Toksoz, 2006, Li et al., 2006), sufficient for constructing preliminary background models. Also, a recent study by Phillips et al. (2007) used *Pn* travel-times to invert for upper mantle velocities and gradients in the region.

Once a suitable set of events, with precise locations of epicenters, depths, and focal mechanisms, is assembled, we will bring together a starting velocity model from published results, including those from recent *Pn* travel-time tomography and seismic refraction studies. In addition, we will incorporate our own results from migration imaging using teleseismic data from the Hi-CLIMB array (Nowack et al., 2007b). We shall then build a large number of seismic profiles based on these chosen events. In the first example (Figure 3), an increase of frequency for *Pn* with propagation distance is already apparent (cf. Boxes A and B in Figure 3), suggesting that the *Pn* from this region is being influenced by interference effects. The next step is to extract seismic attributes from each seismic profile so that quantitative analysis and modeling can be carried out.

The modeling of these attributes involves matching observed envelope-amplitudes and instantaneous pulse frequencies with those calculated, mainly using Gaussian beams. To minimize effects of seismic source-time functions, one strategy is to match pulses observed at close-in distances with theoretical ones and normalize the rest of the data accordingly. Alternatively, the normalization can be performed by deconvolution of all data with an appropriate reference signal. The reference can be a *P*-pulse observed at teleseismic distance, if the event is large enough (m_b above ~5 or 5.5). Otherwise, a pulse observed at close-in distances could be appropriate. Once the seismic attributes are normalized, we will then perform systematic modeling using Gaussian beams. The final product will be several laterally varying velocity and attenuation models over a large region of western China, since numerous regional earthquake from different azimuths were well-recorded by the Hi-CLIMB array (Figure 2).

CONCLUSIONS AND RECOMMENDATIONS

For the first year of this new project, we are building a comprehensive database of regional events recorded by the Hi-CLIMB array. The starting point of this database will be relevant global and regional catalogs of seismicity, followed by relocation of selected events and inversion for source depths and focal mechanisms, if required. The major deliverable will be the database, including the catalog of events with precise locations of epicenters, focal depths, and focal mechanisms. Further validation of the Gaussian beam method is being conducted to efficiently and precisely calculate *Pn* propagation in laterally varying crustal and upper mantle structures. We will carefully compare results from different methods, including those from finite difference algorithms. The comparisons will also include extraction of relevant seismic attributes.

In the second phase of the project, we will construct seismic profiles across the Hi-CLIMB array for a selected set of relocated regional events. Normalization and deconvolution of seismic profiles by various reference signals in order to remove effects of the source-time function will be performed. Extraction of key seismic attributes will then be performed from observed seismic profiles, and detailed modeling/inversion of seismic attributes using Gaussian beams will be conducted in order to build self-consistent models for propagation of *Pn* beneath the Hi-CLIMB array in western China.

REFERENCES

Babich, V. M. and M. M. Popov (1989). Gaussian summation method (review), Radiofizika 32: 1447–1466 (translated in *Radiophysics and Quantum electronics* 32: 1063–1081, 1990).

Braile, L. W. and R. B. Smith (1975). Guide to the interpretation of crustal refraction profiles, *Geophys. J.R. Astr. Soc.* 40: 145–176.

Cerveny, V., M. M. Popov, and I. Psencík (1982). Computation of wavefields in inhomogeneous media—Gaussian beam approach, *Geophys. J.R. Astr. Soc.* 70: 109–128.

Cerveny, V. and R. Ravindra (1971). *Theory of Seismic Head Waves*, Univ. of Toronto Press.

Chen, W.-P., and P. Molnar (1983). Focal depths of intracontinental and intraplate earthquakes and their implications for the thermal and mechanical properties of the lithosphere, *J. Geophys. Res.* 88: 4183–4214.

Chen, W. P. and Z. H. Yang (2004). Earthquakes beneath the Himalayas and Tibet: evidence for strong lithospheric mantle, *Science* 304: 1949–1952.

Clowes, R. M., M. J. Burianyk, A. R. Gorman and E. R. Kanasewich (2002). Crustal velocity structure from SAREX, the Southern Alberta Refraction Experiment, *Can. J. Earth Sci.* 39: 351–373.

Daubechies, I. (1992). *Ten lectures on wavelets*, SIAM, Philadelphia.

Engdahl, E.R., R.D. van der Hilst, and R.P. Buland (1998). Global teleseismic earthquake relocation with improved travel times and procedures for depth determination, *Bull. Seism. Soc. Am.* 88: 722–743.

Gorman A. R., R. M. Clowes, R. M. Ellis, M. J. Burianyk, E. R. Kanasewich, I. Asudeh, Z. Hajnal, G. D. Spence, T. J. Henstock, A. R. Levander, G. R. Keller, and K. Miller (2002). Deep Probe—maging the roots of western North America, *Can. J. Earth Sci.* 39: 375–398.

Hearn, T. M., S. Wang, J. F. Ni, Z. Xu, Y. Yu, and Z. Zhang (2004). Uppermost mantle velocities beneath China and surrounding regions, *J. Geophys. Res.* 109: B11301, doi:10.1029/2003JB002874.

Hill, D. (1971). Velocity gradients and anelasticity from crustal body-wave amplitudes, *J. Geophys. Res.* 76: 3309–3325.

Hill, D. (1973). Critically refracted waves in a spherically symmetric radially heterogeneous earth model, *Geophys. J.R. astr. Soc.* 34: 149–177.

Kao, H., Y.-H. Liu, W.-T. Liang, and W.-P. Chen (2002). Source parameters of regional earthquakes in Taiwan (1999–2000) including the Chi-Chi earthquake sequence, *Terr. Atmos. Ocean. Sci.* 13: 279–298.

Langin, W. R., L. D. Brown, and E. A. Sandvol (2003). Seismicity of central Tibet from Project INDEPTH III seismic recordings, *Bull. Seism. Soc. Am.* 93: 2146–2159.

Li, S., W. D. Mooney, and J. Fan (2006). Crustal structure of mainland China from deep seismic sounding data, *Tectonophysics* 420: 239–252.

Liang, C. and X. Song (2006). A low velocity belt beneath northern and eastern Tibetan Plateau from Pn tomography, *Geophys. Res. Lett.* 44: L22306, doi:10.1029/2006GL027926.

Liang, C., X. Song, and J. Huang (2004). Tomographic inversion of *Pn* travel times in China, *J. Geophys. Res.* 109: B11304: doi:10.1029/2003JB002789.

Lugara, D., C. Letrou, E. Shlivinski, E. Heyman, and A. Boag (2003). Frame-based Gaussian beam summation method: theory and applications, *Radio Science* 38: 8026.

Mallat, S. (1999). *A wavelet tour of signal processing*, 2nd edition, Academic Press, San Diego.

Matheney, M. P. and R. L. Nowack (1995). Seismic attenuation values obtained from instantaneous frequency matching and spectral ratios, *Geophys. J. Int.* 123: 1–15.

Matheney, M. P., R. L. Nowack, and A. M. Trehu (1997). Seismic attribute inversion for velocity and attenuation structure, *J. Geophys. Res.* 102: 9949–9960.

Meissner, R., F. Tilmann, and S. Haines (2004). About the lithospheric structure of central Tibet, based on seismic data from the INDEPTH III profile, *Tectonophysics* 380: 1–25.

Menke, W. H. and P. G. Richards (1980). Crust-mantle whispering gallery phases: a deterministic model of teleseismic Pn wave propagation, *J. Geophys. Res.* 85: 5416–5422.

Molnar, P., and W.-P. Chen (1983). Depths and fault plane solutions of earthquakes under the Tibetan plateau, *J. Geophys. Res.*, 88: 1180–1196.

Morozov, I., E. A. Morozova, S. B. Smithson, and L. N. Solodilov (1998). On the nature of the teleseismic Pn phase observed on the ultralong-range profile Quartz Russian, *Bull. Seismol. Soc. Am.*, 88: 62-73.

Morozov, I. and S. B. Smithson (2000). Coda of long-range arrivals from nuclear explosions, *Bull. Seism. Soc. Am.* 90: 929–939.

Nielsen, L. and H. Thybo (2003) The origin of teleseismic Pn waves: Multiple crustal scattering of upper mantle whispering gallery phases, *J. Geophys. Res.* 108: doi:10.1029/2003JB002487.

Nowack, R. L. (2008). Frame-based Gaussian beam summation and seismic head waves, in *Proceedings of the Project Review*, Geo-Mathematical Imaging Group, Purdue Univ. West Lafayette IN, Vol. 1, 113–119.

Nowack, R. L. (2003). Calculation of synthetic seismograms with Gaussian Beams, *Pure Appl. Geophys.* 160: 487–507.

Nowack, R. L. and K. Aki (1984). The two-dimensional Gaussian beam synthetic method: testing and application, *J. Geophys.* 89: 7797–7819.

Nowack, R. L. and M. P. Mathaney (1997). Inversion of seismic attributes for velocity and attenuation structure, *Geophys. J. Int.* 128: 689–700.

Nowack, R. L. and S. M. Stacy (2002). Synthetic seismograms and wide-angle seismic attributes from the Gaussian beam and reflectivity methods for models with interfaces and velocity gradients, *Pure Appl. Geophys.* 159: 1447–1464.

Nowack, R. L., W.-P. Chen, U. E. Kruse, and S. Dasgupta (2007a). Imaging offsets in the Moho: Synthetic tests using Gaussian beam with teleseismic waves, *Pure Appl. Geophys.* 164: 1921–1936

Nowack, R. L., W.-P. Chen, T. L. Tseng, and the Hi-CLIMB Imaging Team (2007b). Imaging the crust and upper mantle beneath the Hi-CLIMB seismic array in Tibet using Gaussian beam migration of radial receiver functions, Fall 2007 Am. Geophys. Un. Meeting, San Francisco.

Nowack, R. L., S. Dasgupta, G. T. Schuster, and J. M. Sheng (2006). Correlation migration using Gaussian beams of scattered teleseismic body waves, *Bull. Seism. Soc. Am.* 96: 1–10.

Phillips, W. S., M. L. Begnaud, C. A. Rowe, L. K. Steck, S. C. Myers, M. E. Pasyanos, and S. Ballard (2007). Accounting for lateral variations of the upper mantle gradient in Pn tomography studies, *Geophys. Res. Lett.* 34: L14312, doi:10.1029/2007GL029338.

Popov, M. M. (1982). A new method of computation of wave fields using Gaussian beams, *Wave Motion* 4: 85–97.

Popov, M. M. (2002). *Ray theory and Gaussian beam method for geophysicists*, Universidade Federal da Bahia, Brazil, 172 pp.

Ryberg, T., K. Fuchs, A. V. Egorkin, and L. Solodilov (1995). Observation of high frequency teleseismic Pn waves on the long-range Quartz profile across northern Europe, *J. Geophys. Res.* 100: 18,151–18, 163.

Ryberg, T., M. Tittgemeyer, and F. Wenzel (2000). Finite difference modeling of P-wave scattering in the upper mantle, *Geophys. J. Int.* 141: 787–800.

Sereno, T. J. and J. W. Given (1990). Pn attenuation for a spherically symmetric earth model, *Geophys. Res. Lett.* 17: 1141–1144.

Stacy, S.M. and R. L. Nowack (2002). Modeling of wide-angle seismic attributes using the Gaussian beam method, *Studia Geophys. Geod.* 46: 677–690.

Sun, Y. and M.N. Toksoz (2006). Crustal structure of China and surrounding regions from P wave traveltime tomography, *J. Geophys. Res.* 111: B03310, doi:10.1029/2005JB003962.

Taner, M. T., F. Koehler, and R. E. Sheriff (1979). Complex seismic trace analysis, *Geophysics* 44: 1041–1063.

Tittgemeyer, M., F. Wenzel, K. Fuchs, and T. Ryborg (1996). Wave propagation in a multiple scattering upper mantle – observation and modeling, *Geophys. J. Int.* 127: 492–502

Virieux, J. (1988). P-SV wave propagation in heterogeneous media: velocity-stress finite-difference method, *Geophysics* 51: 889–901.

Yang, X., T. Lay, X. B. Xie, and M.S. Thorne (2007). Geometric spreading of Pn and Sn in a spherical earth model, *Bull. Seism. Soc. Am.* 97: 2053–2065.

Zhu, L., Y. Tan, D. V. Helmberger, and C. K. Sikia (2006). Calibration of the Tibetan Plateau using regional seismic waveforms, *Pure Appl. Geophys.* 1193–1213.